Version of Record: https://www.sciencedirect.com/science/article/pii/S0360132321001992
Manuscript_9d21b8e354d3fd29fb082dcd672fe3ed

The Seasonal Microclimate Trends of a Large Scale Extensive Green Roof

Lauren Smalls-Mantey[1] and Franco Montalto[1]

[1]Department of Civil Architectural and Environmental Engineering, Drexel University, 3141 Chestnut Street, Philadelphia, PA 19104, USA

Corresponding Author: Franco Montalto (fmontalto@coe.drexel.edu)
+1-215-895-1385

Funding: This research was funded principally by the Jacob K. Javits Convention Center, with additional support by the National Science Foundation through CAREER: Integrated Assessments of the Impacts of Decentralized Land Use and Water Management (CBET: 1150994), and the National Oceanic and Atmospheric Association (NOAA) through Supporting Regional Implementation of Integrated Climate Resilience: Consortium for Climate Risks in the Urban Northeast (CCRUN) Phase II (NA15OAR4310147)

Acknowledgments: The authors acknowledge the contributions of many members of Drexel University's Sustainable Water Resource Engineering lab in monitoring system installation.

Abstract

At nearly 27,500 m^2, the Jacob K. Javits Convention Center (JJCC) located in New York City, hosts one of the largest extensive green roofs in the United States. This paper explores three years of fine scale microclimate data collected at the JJCC green roof and its potential ability to reduce the urban heat island intensity (UHII). Surface energy fluxes and microclimate parameters on four different surfaces are analyzed before and after installation of the southern section of the green roof, offering a unique before/after, test/control study. The results indicate that the temperatures of the air above the green roof, and its exterior surface are different (e.g. lower) than those measured above and on, respectively, the black roof that preceded it. Differences in the maximum daytime air and surface temperature between the black and green roof were 1.80 °C and 18.4 °C, respectively. Installation of the green roof increased evapotranspiration, modifying the roof's surface energy balance, and reduced the median summer nighttime UHII (compared to the pedestrian level station) by 0.91 °C. Though microclimatic conditions on two sections of the green roofs vary somewhat, the research findings generally support the statement that green roofs are an effective strategy for mitigating the UHI effect.

1. Introduction

Urbanization often involves the replacement of natural landscapes with impervious surfaces, such as roofs and roads. Because the thermal properties of built and natural surfaces differ significantly, urbanization leads to a modification of the urban energy balance, including elevation of urban temperatures above those of otherwise equivalent rural areas, a difference measured in terms of the urban heat island intensity (UHII) [1]. New York City's UHII was found to be as high as 4 °C and 3 °C in the summer/autumn and winter/spring, respectively [11]. Due to the greater relative thermal mass of urban surfaces, and their tendency to release heat more slowly than natural surfaces, the greatest UHII is typically observed from the late afternoon through the night [1,23]. Prolonged frequent nighttime UHIIs are considered risks to human health, since they reduce the amount of time that the body has to recover from daytime high temperatures [29].

To bring about a more sustainable form of urban development, especially in the context of climate change, urban designers are in search of strategies like green (e.g. vegetated) roofs that can alter the local microclimate so as to partially mitigate some of the urban heat island (UHI) effect. Previous work has documented the ability of green roofs to provide thermal buffering, to increase the energy efficiency of building systems, and to reduce their exterior surface and air temperatures [1, 2, 4, 8, 19, 21, 22, 25]. Such processes are mediated through (1) the shade provided by rooftop growing media and plants, (2) convective cooling brought about through the process of evapotranspiration (ET) [25] and (3) reflectance of solar radiation by high albedo leaf surfaces [13]. Research by Peng [17], for example, suggests that green roofs can reduce surface temperatures by 15-45 °C and the near surface air temperature by 2-5 °C. Speak [26] and Susca [27] have also reported cooling reductions in this range. Studies that compare a green roof to a traditional roof structure include Getter [33] which reported air temperature directly above the green roof to be 5 °C lower than white gravel roof temperatures and peak temperature differences reaching as much as 20 °C in the summer. Another study Qin [35], reports the green roof reduced surface temperature and air temperature by an average of 7.3 °C and 0.5 °C, respectively. Jim and Peng [36] reported a 0.7 °C air temperature difference between the original and green roof at 10 cm but did not observe a significant effect at 1.6 m. Alvizuri et al [2], used thermal imaging to quantify the ability of a green roof on top of the Jacob K. Javits Convention Center (NYC) to provide buffer thermal fluxes through the roof, finding that its exterior surface was >16 °C cooler than a black bitumen roof, and 5-10 °C cooler than an adjacent sidewalk surface during the warm months.

Though the body of green roof research is growing, thermal studies often focus on a very limited spatial area [14], are short-term, and do not compare pre- and post- green roof observations [5, 7]. In addition, most green roof thermal research utilizes modeling and not monitoring results, does not investigate the influence of the green roof on street level air temperature, and does not report changes in air temperature before and after installation. The present study fills some of these gaps by studying the microclimate and energy fluxes of a large scale extensive green roof built on top of the Jacob K. Javits Convention Center (JJCC) in New York City (Figure 1), in an attempt to quantify its role in reducing the UHII. It extends the work of Alvizuri et al [2], who quantified the ability of this particular green roof to modify its microclimate. The research utilizes data gathered over three years from four weather stations located on and around the JJCC, beginning before the green roof was installed. The discussion attempts to further practitioner questions regarding whether partially greened roof surfaces can alter the UHII and if the cooling provided by the green roof influences street level air temperatures.

2. Materials and Methods

The JJCC is located on the west side of Manhattan between 34th and 40th streets and between 11th and 12th avenues (Figure 1). The height roof is approximately 56 m above the ground elevation. Its 27,316 m^2 green roof was fully completed during the Spring of 2014 and consists of a Xero Flor XF301 + XT extensive system. In section, it consists of a pre-vegetated sedum mat installed on top of 1.5-5 cm of growing medium, a retention fleece layer, a drainage layer and a root barrier, as described in detail in Alvizuri et al [2]. The JJCC green roof is several stories above the ground surface, on a sloped section of Manhattan's west side.

2.1 Description of Monitoring System

Monitoring of the Javits Green Roof (JGR) was initiated in July 2013, before the south section of the green roof had been completed, enabling a comparison of the pre- and post- green roof installation on the south section. The full monitoring setup was designed to aid in quantifying the energy and water balance of the JGR and includes climate stations, weighing lysimeters, soil sensors, flumes, pressure transducers and an infrared camera. Only the climate stations (Figure 1) and weighing lysimeters (Figure 2) are utilized in the analysis presented here. A thermal flux analysis is published separately in Alvizuri et al [2].

In July of 2013, four climate stations three meters high were positioned (1) on the newly completed, north extensive green roof, hereafter referred to as the "north green roof" (NGR), (2) on the south roof which still had a black asphalt bitumen surface, referred to as the "black roof" (BR), (3) on the metal reflective roof of a separate JJCC building located immediately to the north of the NGR, termed the "metal roof" (MR) and (4) on a light pole mounted above the side walk to the east of the JGR on 11th avenue at street level, referred to as the "street level station" (SLS).

By June 2014, the BR had been converted to an extensive green roof and is thereafter referred to as the "south green roof," (SGR). In this paper the BR refers to the original southern roof which includes all dates before June 2014. All climate stations were installed at a height of approximately three meters over the respective surface and monitored continuously at five-minute intervals. Although the weather station measurements were made only three meters above the surface, a higher section of roof existed at the JJCC and the monitored roofs were at a similar height to many of the roof tops in the vicinity at the time of the analysis. Thus, the observations recorded at the

stations fall within the urban canopy layer. The parameters measured by the climate station and the corresponding equipment specifications are described in Table 1. The albedo and monitoring periods for each surface are presented in Table 2. Each of the 4-component net radiometers were calibrated for the surface using the manufacturers procedure.

To quantify the rate of ET from the JGR, three weighing lysimeters were installed on the SGR (Figure 2). Each lysimeter consists of a square section of green roof, enclosed in a 0.372 m^2 metal box that rests on a custom 0.372 m^2 Rice Lake Roughdeck mild steel platform scale equipped with four mild steel load cells. The maximum capacity of the scale is 227 kg with a 0.02 kg resolution. Although physically isolated from the green roof, the lysimeter is surrounded by four sloped transition sections of the green roof to minimize the boundary effects. The metal box is tilted on the weighing scale at a similar slope as the green roof to allow drainage from the lysimeter.

To quantify the UHII at the JJCC monitoring locations, a fifth weather station was established at a reference site. This climate station, identical in components and sampling frequency, was established in Alley Pond Park (Queens, NY), a 2.7 km^2 urban park containing one of the last sections of old growth forest in New York City. The climate station was installed under the forest canopy (Figure 3). This reference site is a canopied weather station approximating pre-industrial era air temperature conditions.

The monitoring instruments were used to compare air and surface temperatures, compute surface energy fluxes, and to measure the UHII at the four monitoring locations. These methodologies are described below.

2.2 Statistical analysis of air and surface temperatures

The relationships between the air and surface temperature for each surface were evaluated by averaging five-minute measurements over hourly intervals. The temperature measurements were not normally distributed, requiring the use of non-parametric statistical analyses [13] performed in R, version 3.3.1 (Mavericks Build). The Kruskall-Wallis test ($\alpha = 0.05$) was first used to test whether the distributions of air temperature differences were the same (e.g. the null hypothesis) for all climate stations. After rejection of the null hypothesis ($p < 0.05$), pairwise differences in air and surface temperature between the different monitoring locations were computed, and Dunn post hoc tests were used to determine which pairs were statistically similar or different.

2.3 Computation of surface energy fluxes

The main energy fluxes of the surface energy balance over any surface are represented as:

$$Q^* = Q_H + Q_C + Q_{LE}, \quad (1)$$

where Q^* represents the net radiation, Q_H is the sensible heat flux, Q_{LE} is the latent heat flux and Q_C is the conductive heat flux. The sign convention denotes non-radiative flux away from the surface as positive. The *net radiation* (Q^*) was calculated from the four-component radiation measured at the climate station and is expressed as:

$$Q^* = K\downarrow - K\uparrow + L\downarrow - L\uparrow, \quad (2)$$

where K is the shortwave radiation (solar radiation) flux, L is the longwave (terrestrial) radiation flux and the arrows represent the flow of energy toward (↓) or away (↑) from the surface. Q* is an upper bound on the energy that is available to heat the air and ground or to evaporate water [15].

The *sensible heat flux* (Q_H) characterizes the transfer of energy between the surface and the air along a vertical temperature gradient. This heat transfer process is through both conduction (air and surface transfer) and convection (upwards circulation of air). The transfer of sensible heat from the surface into the air or vice versa is driven by the temperature gradient between the air and surface. Positive Q_H values indicate heat transfer to the air, while negative values indicate the opposite.

Ground heat flux (Q_C) (or *conductive heat flux* in the case of the green roof), involves the transfer of heat to the surface from the subsurface through the process of conduction. Q_C is driven by a temperature gradient between the surface and subsurface.

The *latent heat flux* (Q_{LE}) is the consequence of the phase change of liquid water to vapor. The energy required for this phase change is termed the latent heat of vaporization and is used to convert depth averaged ET rates into energy flux equivalents as follows:

$$Q_{LE} = \lambda_v ET, \quad (3)$$

where is the latent heat of vaporization and ET is the evapotranspiration rate [LT^{-1}]. The ET was calculated using the mass changes from the lysimeter based on equation 4:

$$ET = \sum_{i=1}^{x} \left(\frac{m_i - m_{i+1}}{A\rho}\right)_i, \quad (4)$$

where ET is the evapotranspiration, *mi* and *mi+1* are the mass of the lysimeter at consecutive sampling intervals, *x* is the number of sampling intervals, Δt is the time between sampling intervals, ρ is the density of water and *A* is the surface area of the weighing lysimeter open to ET. To minimize the potential for errors due to gravity-driven vertical discharge of water out of the bottom of the lysimeter, ET values were only calculated more than 24 hours after a precipitation event.

To quantify the amount of energy available to heat the air and surface (after any ET had occurred), the *'residual energy flux'* (RSE) is defined as follows:

$$RSE = Q^* - Q_{LE} = Q_H + Q_C. \quad (5)$$

Specifically, the RSE represents the energy available for Q_H and Q_C, the two processes that can bring about a local temperature change. Because no ET measurements were performed within 24 hours of a rain event and no there is no ponding on the surface, we assume negligible latent heat flux ($Q_{LE} \sim 0$) on non-vegetated surfaces (i.e. SLS, BR, MR). Unfortunately, Q_{LE} could not be computed for the NGR because there is no lysimeter present on this section of the roof. Previously published research presents the measured heat fluxes through the roof layers [2]. The heat accumulation term could not be directly measured in this study but is included cumulatively with the RSE.

2.4 Computation of the UHI intensity

The UHII was calculated as the air temperature difference between the monitoring station and the rural reference station, Alley Pond Park, and was represented as follows:

$$UHII = T_J - T_{AP}, \quad (6)$$

where T_J represents any of the four climate station locations on and around the Javits Center, and T_{AP}, is the simultaneous temperature measured at Alley Pond Park.

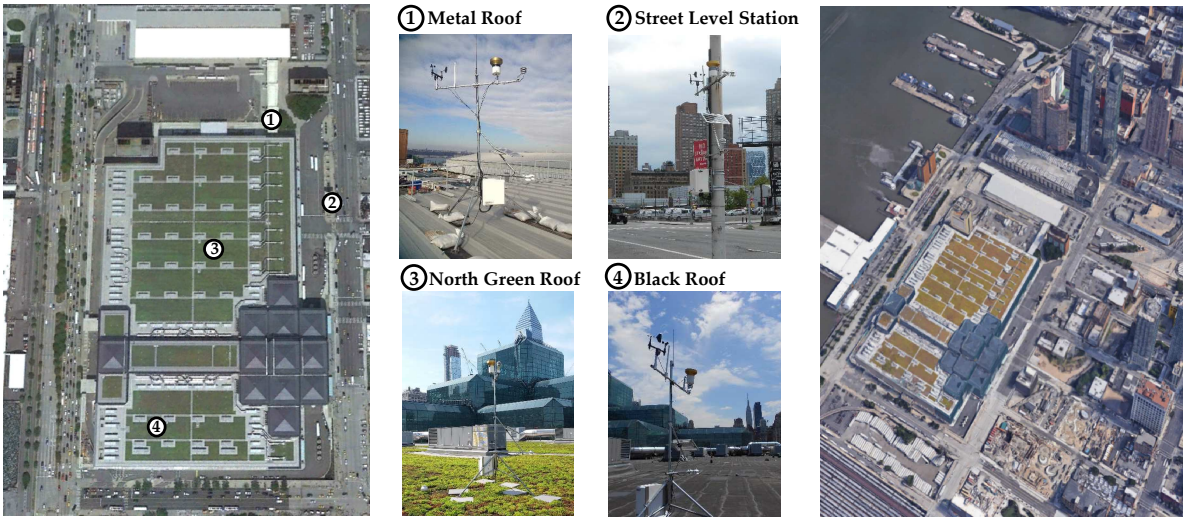

Figure 1: Climate station locations and monitored surfaces at the Jacob K. Javits Convention Center (Google, 2017)

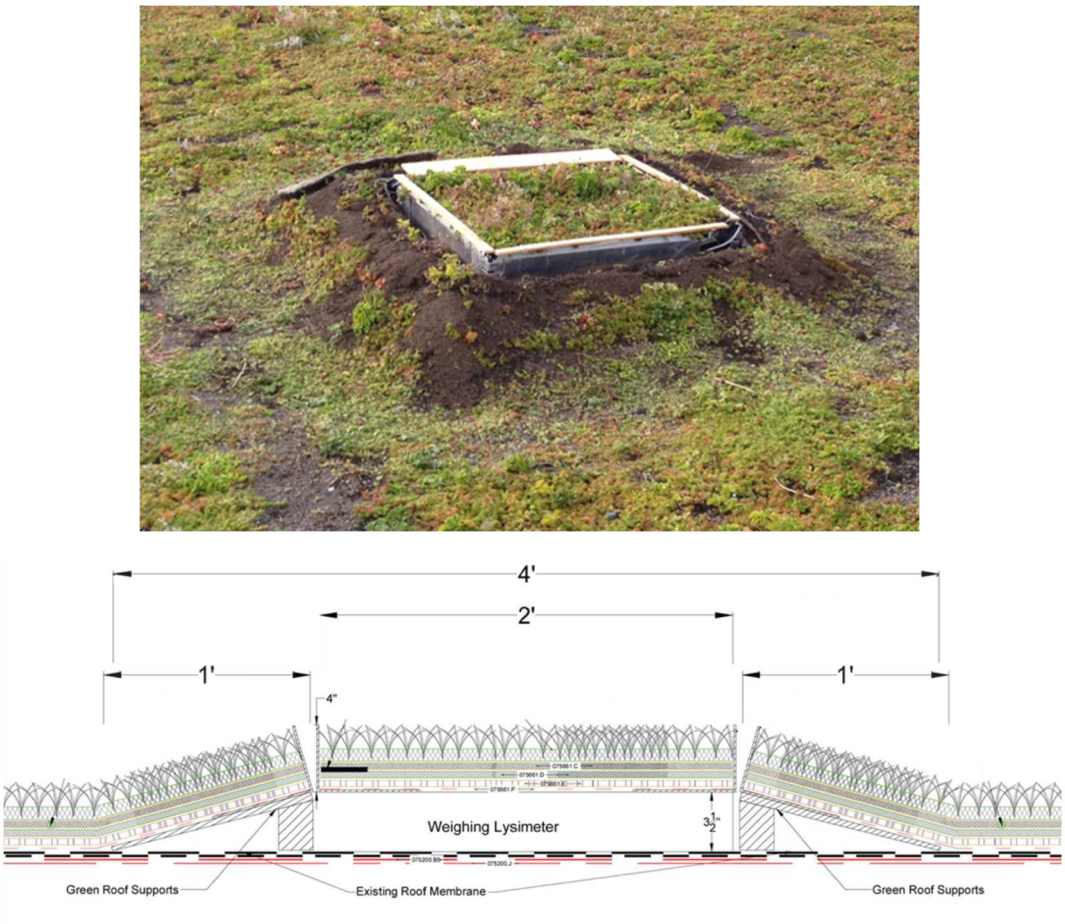

Figure 2: JJCC weighing lysimeter located on the SGR**.** Top: Picture of lysimeter installed on the roof; Bottom: Cross-section drawing of lysimeter

Figure 3: Image of Alley Pond Park climate station

Measured Parameter	Equipment	Sensor Accuracy
Logger	Campbell Scientific CR1000	Logged at 5 min intervals
	Climate Station	
Precipitation	Texas Electronics, Inc. Series 525 Rainfall Sensor	1.0% at 10 mm/hr or less
Wind Speed and Direction	Model 5103 - Young Wind Sentry Anemometer	Anemometer: ±0.5 m/s Vane: ±5°
Longwave Radiation (In/Out) Shortwave Radiation (In/Out)	Hukseflux NR01 4-Compnemnt net-radiation sensor	±10 %
Air Temperature and Relative Humidity	Campbell Scientific CS215	Air Temperature: ±0.3 °C Relative Humidity: ±4%
Surface Temperature	Hukseflux NR01 4-Compnemnt net-radiation sensor	±20 %
Evapotranspiration	Custom 0.372 m^2 Lysimeter	---

Table 1: Climate station equipment and sensor accuracy

Table 2: Surface monitoring periods and albedo

Surface Type	Monitoring Period Analyzed	Shortwave Surface Albedo[a]
Metal Roof (MR)	Jul 2013- Dec 2016	0.39
Street Level Station (SLS)	Jul 2013-Dec 2016	0.16
North Green Roof (NGR)	Jul 2013- Dec 2016	0.22
Black Roof (BR)	Aug 2013- Nov 2013	0.13
South Green Roof (SGR)	Jun 2014- Dec 2016	0.21
Alley Pond Park (forest floor)	Jul 2014- Dec 2016	0.24

[a] Calculated as the ratio of shortwave observations from the NR01 radiometer

3. Results and Discussion

This study presents an examination of the microclimate and energy fluxes above four different surfaces on and around a large-scale green roof, pre and post installation. The surfaces included a concrete sidewalk, a traditional urban metal roof, a black roof, and the green roof. The results serve as an exploration into how these kinds of urban surfaces may contribute to the warming of the urban environment assuming the partitioning of energy into Q_{LE} leaves less energy available for Q_H, reducing the transfer of thermal energy to the atmosphere.

3.1 Analysis of air temperature

A microclimate summary of the four monitoring sites and hourly temperature anomalies between the respective monitored station and NGR is presented in Figure 4. The results of the non-parametric post hoc analysis of all the monitored station pairs (Figure 5) are displayed using the following color scheme: (1) shaded red (e.g. true) indicating a failure to reject the H_0, meaning that the two observed air temperatures were similar and (2) shaded blue (e.g. false) indicating a rejection of H_0, meaning that the air temperatures of the pair were different.

As expected, the air temperature above the BR was significantly higher than the air temperature above the NGR. The maximum daytime air temperature difference between the black and green roof was recorded as 1.80 °C. This is different from the results in Jim and Peng [36], which did not observe air temperature differences greater than one meter above the surface. The smallest temperature anomaly was observed between the SGR and NGR, indicating the similarity of air temperature for the two green roofs. However, the SGR air temperature was consistently slightly higher than the NGR, even during the summer months. This observation could be attributed to orientation of the building relative to the cardinal directions (e.g. greater solar gain on the south side of the building).

The MR station was located on a roof surface between two buildings and the SLS station at street level to the east of the green roof. However, even though the strongest wind speed was observed at the MR station, the SLS and MR maintain similar air temperature profiles.

Significance analysis indicates similar air temperature between all the stations during the winter and spring months, a period which also corresponds to when the sedum is dormant. Outside of these months (summer and autumn), air temperature anomalies compared to the NGR were observed to be significantly different, with only two exceptions involving the comparison of NGR to SGR for two summer months (7/2014, 5/2015). Interestingly, although the SLS and MR present different surface and environmental conditions, their air temperatures do not differ significantly for all months except 12/2013.

The differences displayed in Figure 4 highlight the potential importance of changes in energy fluxes (i.e. evapotranspirative cooling) on air temperature. The results presented in Figure 4 and 5 suggest that the cooled air atop the green roof may not reach street level.

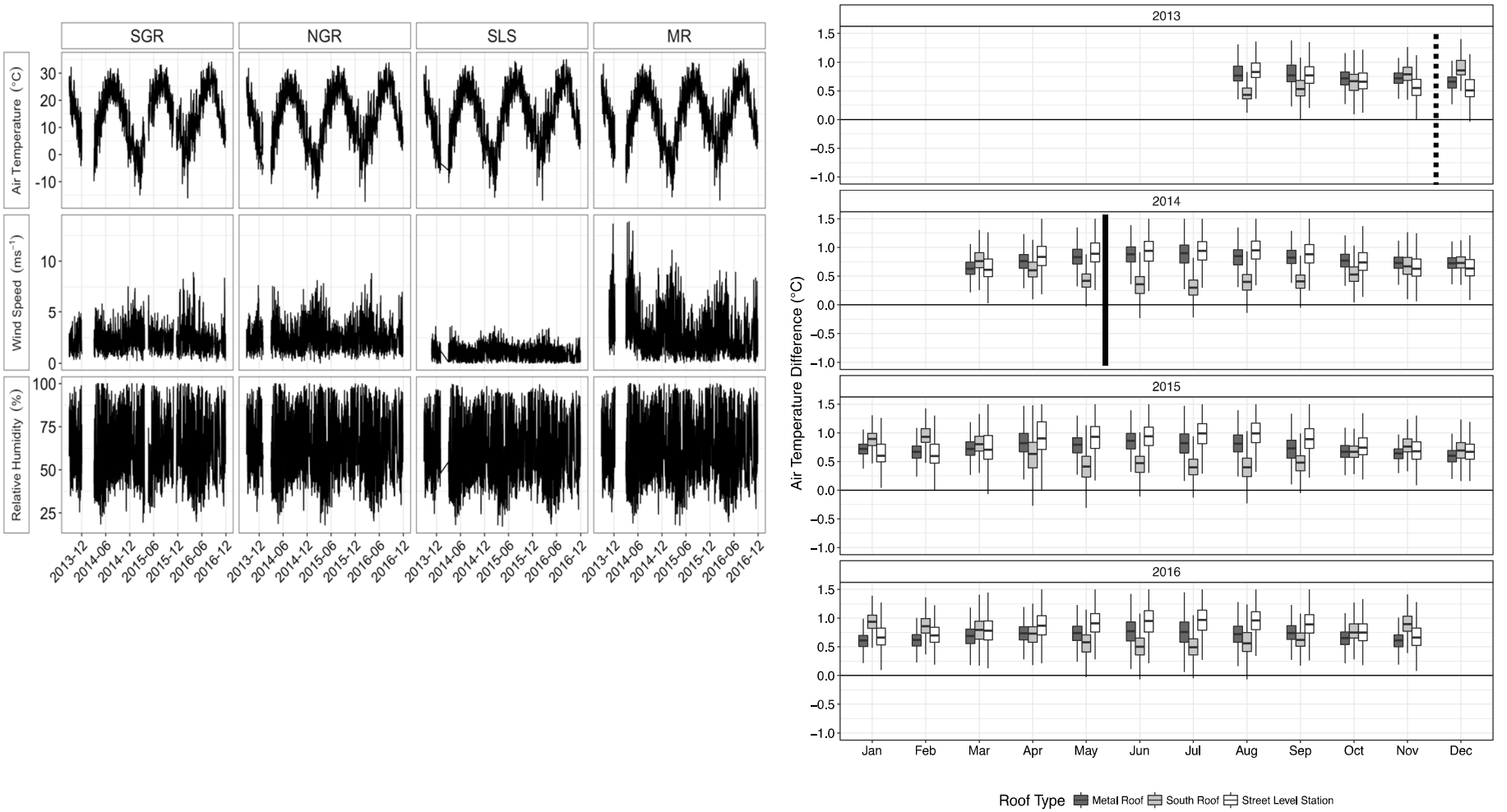

Figure 4: *Left:* Microclimate summary and air temperature anomaly profiles. *Right*: Monthly median air temperature differences from NGR. Note: The dotted and solid line denote the beginning end of the SGR installation, respectively.

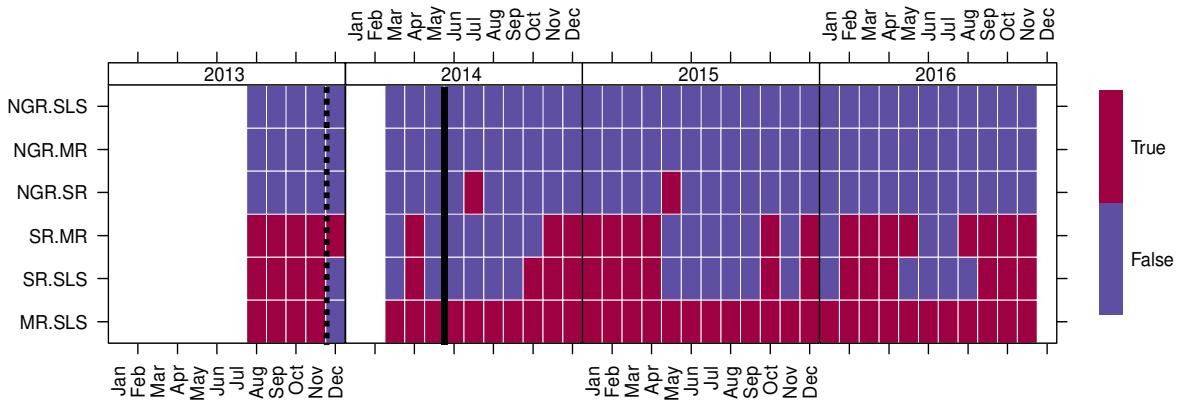

Figure 5: Air temperature post-hoc test results of surface pairs per month. True = fail to reject H_0, False = reject H_0. The dotted and solid line denote the beginning end of the SGR installation, respectively.

3.2 Analysis of surface temperature

The average hourly surface temperatures at each location versus the surface temperature of the NGR, per season is displayed in figure 6. To facilitate visualization of diurnal variations, the observations are colored based on the hour of the day. During the day, the surface of the BR was consistently higher than the surface of the NGR, especially in the afternoon, and it rarely fell below the surface temperature of the NGR at any time of the day. Unlike the other surfaces, the BR surface remained warmer for longer during the day. After the completion of the SGR, the surface temperature on the two green roof surfaces were nearly identical, with only a few summer daytime periods as exceptions.

In general, during the summer, maximum daytime surface temperatures differed from the NGR as follows (positive values are exceedances): BR, 12.07 °C (9/2013); SLS, 9.53 °C; MR, -22.15 °C. Notably the surface of the SGR and NGR differed by a maximum of 3.81°C and 2.88 °C, in spring and autumn, respectively. Compared to the other surface temperature anomalies the difference is relatively small.

While diurnal surface temperature trends displayed by the NGR and SGR roof surfaces were similar, profile comparisons with the remaining surfaces were distinctly different. On a typical green roof (i.e. NGR/SGR) during the day radiant energy is absorbed into the surface and released as the sun sets. The black roof maintains a higher surface temperature and experiences wider temperature fluctuations than the NGR only returning to similar surface temperatures during the late night to early morning time period. This supports the findings of Alvizuri et al [2], who concluded that the NGR is a better thermal regulator than the BR. It also upholds the observations in the previous section which showed the BR maintaining a higher air temperature than NGR. However, higher air temperature anomalies do not always translate to higher surface temperatures.

The MR nearly always maintains a lower surface temperature than the NGR through all seasons. The magnitudes of surface temperature between these two surfaces are most divergent at cooler temperatures. In contrast, the SLS only maintains a higher surface temperature than the NGR during the early morning to afternoon time period for all seasons. Recalling the previous section, the air temperature profile SLS and MR are statistically similar, but the MR consistently maintains a lower surface temperature than the SLS and green roofs. This observation can be attributed to the reflective properties of MR which reradiates the incoming radiant energy into the atmosphere, which is further discussed below. It should also be noted that this building serves as a connector or "link" between two buildings but is not thermally regulated inside. The SLS exhibits the most dynamic surface temperature profile compared to the NGR. The interactions between the air and surface are further explored in the next section.

In summary, the surface temperature on the BR was nearly always greater than the NGR. The median and maximum daytime autumn surface temperature differences reached 3.26 °C and 18.4 °C respectively. Gaffin [16] reported a daily average and maximum (peak summer) BR to green roof surface temperature difference of 9.9 °C and 33 °C, respectively, on an extensive green roof in NYC. However, Gaffin's measurements were made in the summer, while ours were during the autumn, a potential explanation for this discrepancy. Hein [34] an Jim [36] observed a maximum surface temperature difference between the green roof and original surface of 18 °C and 11 °C , respectively. The maximum BR and NGR surface temperature difference measurements on the Javits roof was observed as 18.4 °C, similar to observations reported in Hein [37].

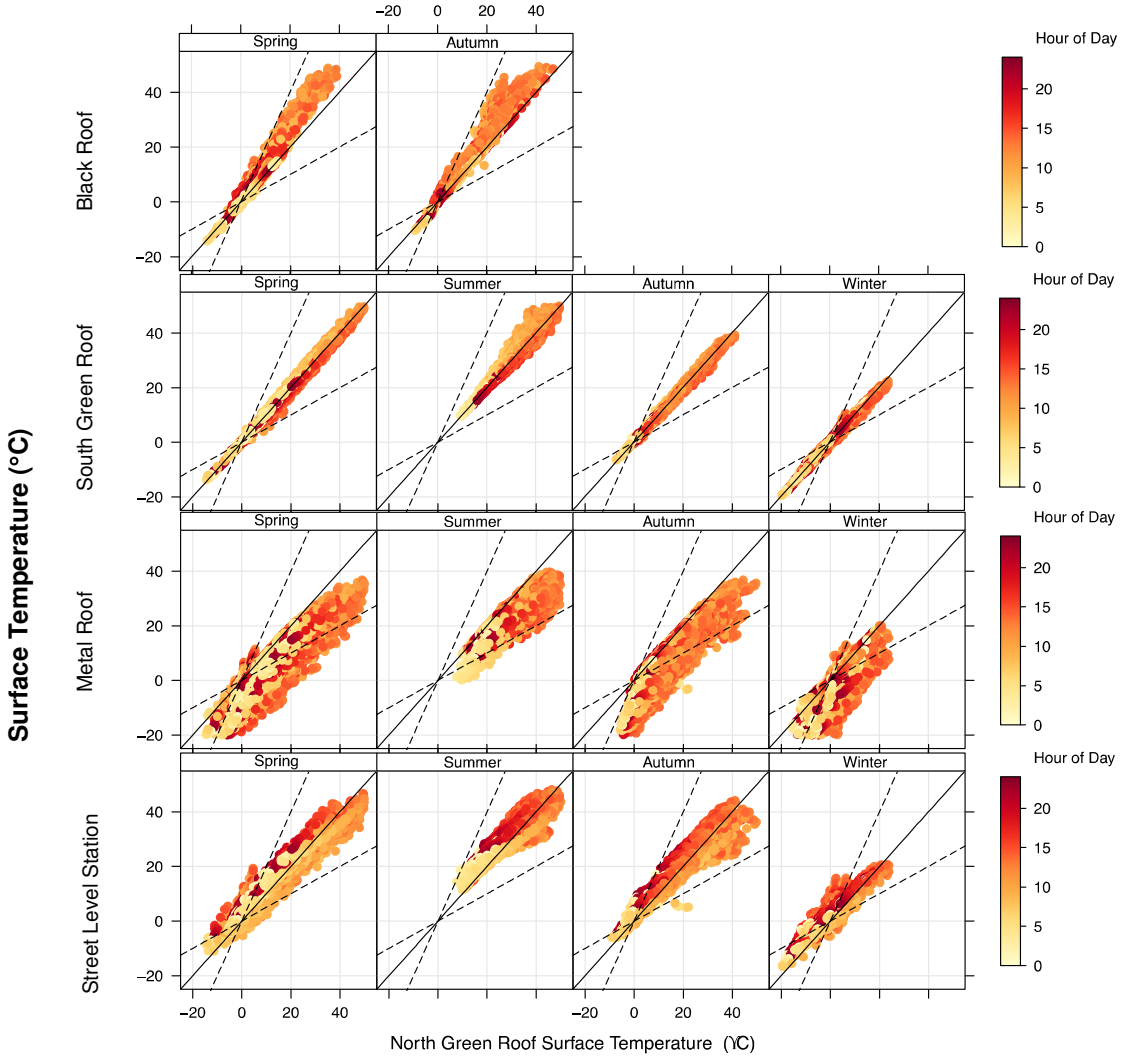

Figure 6: Hourly surface temperature comparisons between the NGR and other monitored surfaces; solid line= 1:1 line; broken line = (right) 1:0.5 (left) 1:2. The colors represent the hour of day.

3.3 Analysis of the Residual Energy Flux

The RSE of the BR, SGR, MR and SLS are shown in Figure 7. Note that the measurements on the south roof were conducted pre- and post-green roof installation. The observations displayed thus represent comparative seasons, but not necessarily the same days. Measurements of Q_{LE} were not calculated in the winter due to the extended freezing conditions in the lysimeter.

The conversion of the BR to the SGR contributed to a 50%, 35% and 56% decrease in the median daytime RSE, for the spring, summer and autumn season, respectively. The highest RSE during the day was displayed by the SLS, followed by the MR and SGR. The RSE of the BR could only be computed for one season, due to the transition from the BR to SGR. Although the UHII on the MR was statistically similar to the SLS, the RSE of the MR was 30%, 37% and 22% less than the SLS for the spring, summer and autumn seasons, respectively.

The largest daytime air temperature was, unsurprisingly, observed on the BR. The lesser transfer of Q_H to the air from the two green roofs, relative to the BR as displayed in Figure 6, suggests that the green roofs do contribute less to warming of the environment.

Installation of the green roof reduced the surface and air temperature on both sections of the JJCC roof. This finding is consistent with previous investigations into microclimatic conditions on the JJCC green roofs conducted using an infrared camera [2]. The green roof decreased the RSE ($Q_H + Q_C$) by 68% in the summer, compared to the BR. Based on equation 1 and the representation of RSE in equation 5, a higher Q_{LE} is attributed to lower RSE. The Q_{LE} at peak solar radiation (midday) during the summer was 364 W m^{-2}. Similar values are reported in literature for other extensive green roofs, as detailed in Table 3 (adapted from [24]) even during the initial summer of the green roof. Increased partitioning of energy into Q_{LE} reduces the RSE, thereby reducing the thermal transfer of energy in the air. The reduced energy transfer into the atmosphere is expressed as lower air temperatures observed directly above the green roof, as observed on the Javits roof between the BR and green roof surfaces.

Large differences in the air temperature between the two green roofs were not observed. However, during most of the monitoring period the SGR consistently displayed higher air temperatures than NGR. This discrepancy could be due to one or more of the following: (1) a slightly longer exposure to solar radiation (e.g. southern solar exposure), (2) differences in the density and maturity of vegetation on the NGR and SGR (i.e. differences in green roof age), or (3) differences in the amount of water available for ET on the SGR. In support of the latter explanations, air temperatures over the SGR differed most from the MR and SLS locations during the sedum's growing season, a potential indicator of the role that vegetation-mediated ET (Q_{LE}) in determining air temperature. Precise differences in ET between the NGR and SGR could not be computed, however, because Q_{LE} was only measured on the SGR.

The largest daytime air temperature was unsurprisingly observed on the BR. The lesser transfer of Q_H to the air from the two green roofs, relative to the BR as displayed in Figure 7, suggests that the green roofs do contribute less to warming of the environment.

Figure 7: Residual energy flux (RSE) diurnal profile of the JJCC monitored locations per season

Table 3: Latent heat from sedum extensive green roofs (Adapted after: Santamouris [24])

Reference	Peak Solar Radiation (Wm^{-2})	Q_{LE} (Wm^{-2})
Feng [10]	900	600
Rezaei [20] and Berghahe [6]	--	350
Marasco [12]	--	USPS: 439 Columbia: 408
DiGiovanni [9]	914	310
Current study	917	364

3.4 Analysis of surface/air temperature rate of change

Typically, the UHII is most prevalent during the late afternoon/evening period and its intensity is due to the type of surface and how energy enters and exits the surface. Figure 8 presents the diurnal rate of change (roc) of air temperature (left) and surface temperature (right) of the four surfaces. A surface with a high positive rate of change absorbs heat faster while a surface with a high negative rate of change denotes heat leaving the surface quickly. The black roof is not shown.

The magnitude of the roc of the air temperature is smaller than the roc surface temperature. Air temperature roc varied most between the surfaces in the morning after sunrise and in the late afternoon during the summer. The air temperature roc of the green roofs begins to decrease earlier than MR and SLS. Also of note is the slope of the line between 16:00 and sunrise (~5:00) in each of the plots. As the seasons progresses into cooler temperatures the slope gets smaller and closer to zero. Interestingly, the

two green roofs, built about a year apart, maintain a similar roc temperature profile although the air temperature on the two roofs are statistically different for a majority of the monitored months. This finding supports the theory that the SGR maintains a slightly higher air temperature than the NGR due to its geographic orientation with respect to solar exposure.

The surfaces of the green roofs warm faster than MR and SLS, but the green roofs also cool faster after sunset. The MR releases heat at lower roc than the green roofs. In the context of UHI formation a slower release of heat is not a favorable. At night the slope of the line is nearly zero. The SLS and MR air temperatures were significantly similar (section 3.1). Interestingly, during the spring and summer at the SLS the surface temperature is always greater than the corresponding air temperature, indicating a transfer of energy from the surface to the atmosphere. During the spring and summer, the surface temperature at the SLS is nearly always greater than the air temperature. However, in autumn this pattern changes. At lower air temperatures, the surface temperature is greater than the air for most of the day. At higher air temperatures this pattern is only exhibited during the day. These observations have led to the belief there is a tunnel under the SLS as the presence of a void would change the surface/air dynamics of the surface.

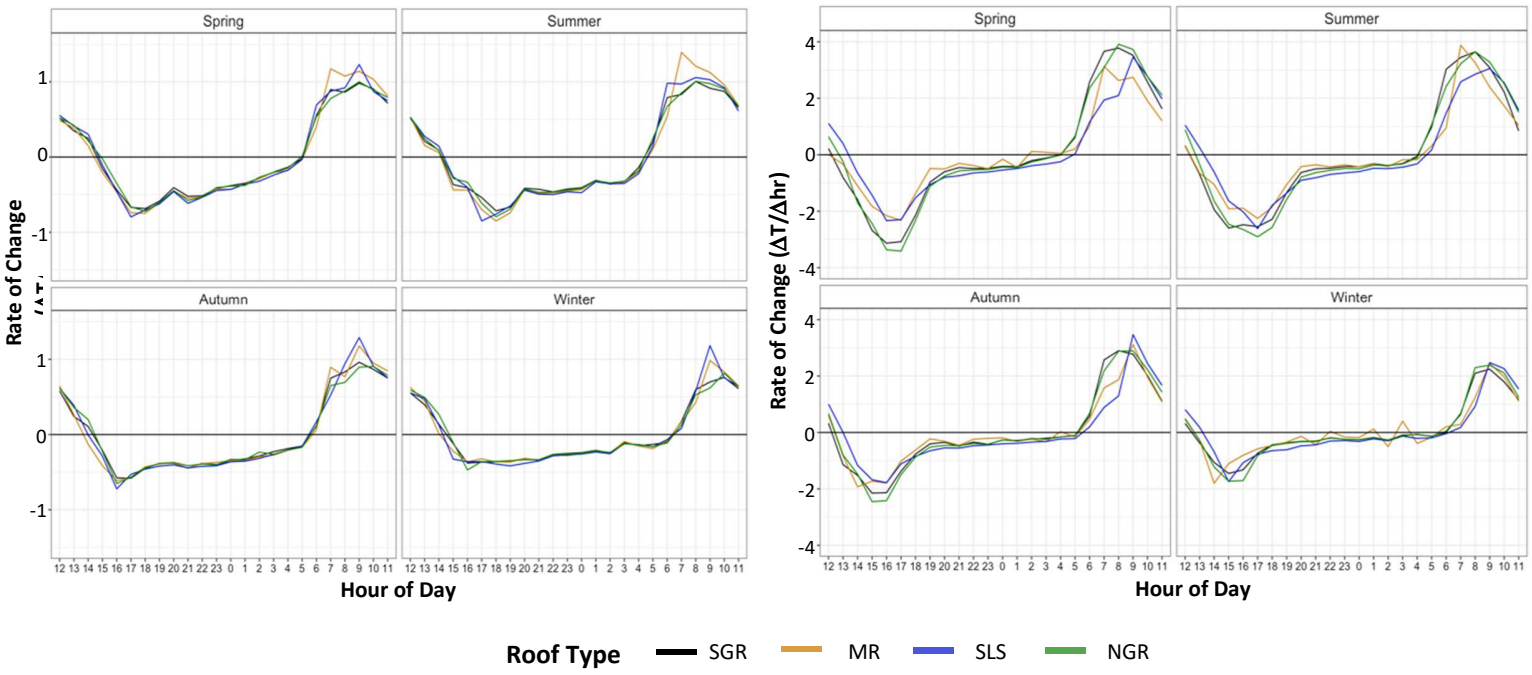

Figure 8: Rate of Change diurnal profile- Left: air temperature; Right: surface temperature; SS: sunset; SR: sunrise

3.5 Analysis of the UHII

Figure 9 displays the diurnal variation in the UHII at each monitoring location, by season. Only the data collected after completion of the SGR (e.g. between November 2014 to May 2016) are included in this analysis. Clear diurnal patterns are observed, with the lowest UHII observed at mid- day (12h) and the highest between sunset and sunrise.

The statistical significance of the daytime and nighttime UHII per season is displayed in Figure 10. Boxes shaded red (H_0 = true) indicate that the two observed UHII values were similar. Boxes shaded blue (H_0 = false) indicate that the UHII pairs were different. Regardless of time of day, the NGR UHII was significantly lower than all the other surfaces. By contrast, the UHII at the SGR was not significantly different from the MR and SLS during two specific periods: (1) at night during the spring and autumn season and, (2) during winter daytime hours. The UHII of the MR and SLS locations were generally similar, except during the winter season.

Maximum and median UHII measurements for daytime and nighttime periods are displayed per season in Table 4. Across all seasons and times of the day the max UHII on the NGR 0.88 °C less than the SLS. The NGR's peak UHII is more than 1 °C less than the SLS during the spring daytime and nighttime hours, as well as the summer nighttime hours.

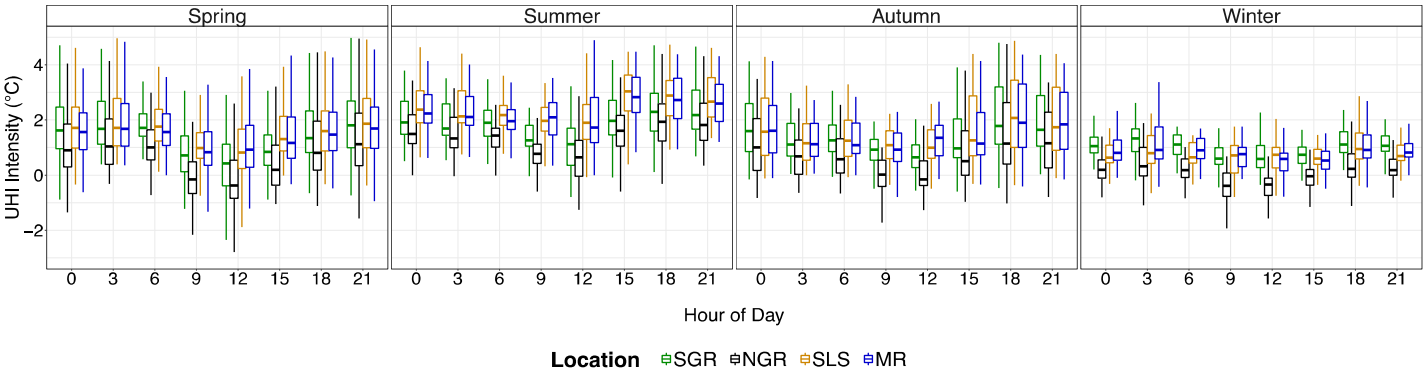

Figure 9: UHII profile of all JJCC monitoring locations, per season. Reference site: Alley Pond Park

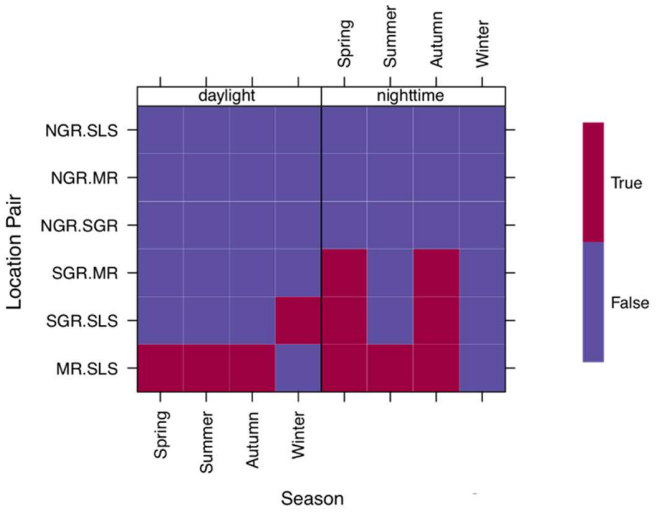

Figure 10: Air temperature post-hoc test results- True = fail to reject H_0, False = reject H_0. Shaded regions indicate statistical similarity among shaded roof types, $\alpha = 0.05$.

Table 4: Median and maximum seasonal UHII observations. Reference site: Alley Pond Park

UHII Period	Maximum (°C)				Median (°C)			
	NGR	*SGR*	*MR*	*SLS*	*NGR*	*SGR*	*MR*	*SLS*
Spring (Day**time**)	8.55	8.77	9.54	9.63	0.268	1.01	1.24	1.29
Spring (Nighttime)	6.04	6.24	6.87	7.13	1.03	1.70	1.70	1.80
Summer (Day**time**)	6.15	6.96	6.71	7.13	1.20	1.68	2.25	2.29
Summer (Nighttime)	5.15	5.40	5.99	6.19	1.56	2.00	2.37	2.47
Autumn (Day**time**)	5.46	5.58	5.78	6.04	0.347	1.02	1.38	1.25
Autumn (Nighttime)	4.71	5.43	5.28	5.41	0.801	1.38	1.43	1.44
Winter (Day**time**)	1.88	3.07	2.66	2.72	-0.191	0.734	0.610	0.749
Winter (Nighttime)	3.87	4.57	4.77	4.65	0.211	1.11	0.878	0.746

Conclusions

This study quantified the differences in observed air and surface temperatures over various urban surfaces (including a green roof). Significant air temperature variability even on two different green roof sections was observed. This observation is important for example in the context of urban planning and modeling which normally assumes a continuous air temperature distribution across the roof.

The addition of the NGR reduced the UHII (compared to the SLS) by 1.1 °C and 0.91 °C for the median summer daytime and nighttime hours, respectively. The SGR reduced temperatures slightly less at 0.48 °C and 0.44 °C for the median summer daytime and nighttime hours, respectively. This effect is attributed to the green roof's role in partitioning more incoming energy into Q_{LE}, which does not require a temperature change, preventing the energy from being converted into Q_H and Q_C, which are fluxes driven by a vertical temperature gradient. Results show that surfaces can vary diurnally and seasonally. When conducting remote studies, care should be taken when analyzing results on land surface types (i.e. side walk, street, reflective roof)

The reduction of the local UHII can be achieved through the implementation of green roofs to meet climate change adaptation needs. The NGR on the JJCC significantly reduced peak daytime air temperatures by 1.7 °C. However, the performance of the green roof is dependent on the plants ability to convert incoming energy into Q_{LE}. Despite only half of the JJCC roof being green through the beginning of the monitoring period, cooling was observed directly on top of the roof. However, either due to the height of the building, in which cooler air is advected down to the pedestrian level or prevailing wind direction, which was towards the west side of the building, cooling effects at the street level could not be observed. This observation is validated by the similar air temperature results at the SLS before and after the SGR installation.

Roofs represent approximately 30-35% of the total land area of the urban environment [30,31]. Therefore, because of its large footprint in the urban environment, many major cities have developed sustainability plans that include a provision allocating the use of this space. For example, NYC has passed Local Laws 92 and 94 which allocates the use of roof space on any roof undergoing "major constriction" to include either a roof with plants, solar panels and/or mini wind turbines. However, in an old, building-dense city such as NYC there are fewer opportunities for new construction outside of replacing the current roof membrane thus many of the NYC's future green roofs will most likely be from an incentive program. Nevertheless, the city will continue to be a mix of traditional and non-traditional roof surfaces at least for the upcoming decade. The data presented in this paper presents a snapshot of the current representation of roof space in the city; the traditional adjacent to the non-traditional. This view is not always captured in models representing high percentage greening scenarios.

References

1. Alexandri, Eleftheria, and Phil Jones. "Temperature decreases in an urban canyon due to green walls and green roofs in diverse climates." *Building and Environment* 43.4 (2008): 480-493.

2. Alvizuri, J., et al. "Green Roof Thermal Buffering: Insights derived from fixed and portable monitoring equipment." Energy and Buildings (2017).

3. ArabI, RoozbeH, et al. "Mitigating Urban Heat Island Through Green Roofs." Current World Environment 10. Special Issue 1 (2015) (2015): 918-927.

4. Berardi, Umberto, AmirHosein GhaffarianHoseini, and Ali GhaffarianHoseini. "State-of-the-art analysis of the environmental benefits of green roofs." Applied Energy 115 (2014): 411-428.

5. Bowler, Diana E., et al. "Urban greening to cool towns and cities: A systematic review of the empirical evidence." Landscape and urban planning97.3 (2010): 147-155.

6. Berghage, Robert, et al. "Quantifying evaporation and transpirational water losses from green roofs and green roof media capacity for neutralizing acid rain." National Decentralized Water Resources Capacity Development Project (2007).

7. Clark, Corrie, Brian Busiek, and Peter Adriaens. "Quantifying thermal impacts of green infrastructure: Review and gaps." Proceedings of the Water Environment Federation 2010.2 (2010): 69-77.

8. Coutts, Andrew M., et al. "Assessing practical measures to reduce urban heat: Green and cool roofs." Building and Environment 70 (2013): 266-276.

9. DiGiovanni, Kimberly, et al. "Applicability of classical predictive equations for the estimation of evapotranspiration from urban green spaces: green roof results." Journal of Hydrologic Engineering 18.1 (2012): 99-107.

10. Feng, Chi, Qinglin Meng, and Yufeng Zhang. "Theoretical and experimental analysis of the energy balance of extensive green roofs." Energy and buildings 42.6 (2010): 959-965.

11. Gedzelman, S. D., et al. "Mesoscale aspects of the urban heat island around New York City." Theoretical and Applied Climatology 75.1 (2003): 29-42.

12. Marasco, Daniel E., et al. "Quantifying evapotranspiration from urban green roofs: A comparison of chamber measurements with commonly used predictive methods." Environmental science & technology 48.17 (2014): 10273-10281.

13. Wong, Nyuk Hien, et al. "Investigation of thermal benefits of rooftop garden in the tropical environment." Building and environment 38.2 (2003): 261-270.

14. Sismanidis, Panagiotis, Iphigenia Keramitsoglou, and Chris T. Kiranoudis. "A satellite-based system for continuous monitoring of surface urban heat islands." Urban Climate 14 (2015): 141-153.

15. Oke, T. R. (1987). Boundary Layer Climates, Routledge, 2nd edition.

16. Gaffin, SR, et al. "A temperature and seasonal energy analysis of green, white, and black roofs." Center for Climate Systems Research, Columbia University, New York, Technical Report (2010).

17. Peng, Lilliana LH, and C. Y. Jim. "Green-roof effects on neighborhood microclimate and human thermal sensation." Energies 6.2 (2013): 598-618.

18. Pohlert, Thorsten. "The pairwise multiple comparison of mean ranks package (PMCMR)." R package (2014): 2004-2006.

19. Niachou, Aikaterini, et al. "Analysis of the green roof thermal properties and investigation of its energy performance." Energy and buildings 33.7 (2001): 719-729.

20. Rezaei, Farzaneh, et al. "Evapotranspiration rates from extensive green roof plant species." 2005 ASAE Annual Meeting. American Society of Agricultural and Biological Engineers, 2005.

21. Scherba, Adam, et al. "Modeling impacts of roof reflectivity, integrated photovoltaic panels and green roof systems on sensible heat flux into the urban environment." Building and Environment 46.12 (2011): 2542-2551.

22. Solecki, William D., et al. "Mitigation of the heat island effect in urban New Jersey." Global Environmental Change Part B: Environmental Hazards 6.1 (2005): 39-49.

23. Rizwan, Ahmed Memon, Leung YC Dennis, and L. I. U. Chunho. "A review on the generation, determination and mitigation of Urban Heat Island." Journal of Environmental Sciences 20.1 (2008): 120-128.

24. Santamouris, Mattheos. "Cooling the cities–a review of reflective and green roof mitigation technologies to fight heat island and improve comfort in urban environments." Solar energy 103 (2014): 682-703.

25. Virk, Gurdane, et al. "Microclimatic effects of green and cool roofs in London and their impacts on energy use for a typical office building." Energy and Buildings 88 (2015): 214-228.

26. Speak, A. F., et al. "Reduction of the urban cooling effects of an intensive green roof due to vegetation damage." Urban Climate 3 (2013): 40-55.

27. Susca, T., S. R. Gaffin, and G. R. Dell'Osso. "Positive effects of vegetation: Urban heat island and green roofs." Environmental Pollution 159.8 (2011): 2119-2126.

28. Takebayashi, Hideki, and Masakazu Moriyama. "Surface heat budget on green roof and high reflection roof for mitigation of urban heat island." Building and Environment 42.8 (2007): 2971-2979.

29. Block, Annie Hunter, Stephen J. Livesley, and Nicholas SG Williams. "Responding to the urban heat island: a review of the potential of green infrastructure." Victorian Centre for Climate Change Adaptation Research Melbourne (2012).

30. “Urban Roofscapes: Using ‘Wasted’ Rooftop Real Estate to an Ecological Advantage.” Scientific American, Scientific American, 25 July 2008, www.scientificamerican.com/article/urban-roofscapes-ecofriendly-rooftops/.

31. Onmura, Sadayuki, M. Matsumoto, and S. Hokoi. "Study on evaporative cooling effect of roof lawn gardens." Energy and buildings 33.7 (2001): 653-666.

32. Carter, Timothy, and C. Rhett Jackson. "Vegetated roofs for stormwater management at multiple spatial scales." Landscape and urban planning 80.1-2 (2007): 84-94.

33. Getter, Kristin L., et al. "Seasonal heat flux properties of an extensive green roof in a Midwestern US climate." Energy and Buildings 43.12 (2011): 3548-3557.

34. Hien, Wong Nyuk, Tan Puay Yok, and Chen Yu. "Study of thermal performance of extensive rooftop greenery systems in the tropical climate." Building and Environment 42.1 (2007): 25-54.

35. Qin, Xiaosheng, et al. "A green roof test bed for stormwater management and reduction of urban heat island effect in Singapore." British Journal of Environment and Climate Change 2.4 (2012): 410-420.

36. Jim, Chi Yung, and Lilliana LH Peng. "Weather effect on thermal and energy performance of an extensive tropical green roof." Urban Forestry & Urban Greening 11.1 (2012): 73-85.